2023 IEEE International Conference on Robotics and Automation (ICRA 2023)
May 29 - June 2, 2023. London, UK

Reconfigurable Inflated Soft Arms

Nam Gyun Kim[1] and Jee-Hwan Ryu[2]

Abstract— **Inflatable structures have attracted considerable research attention in many fields owing to their numerous advantages, such as being light and able to engage in interactions safely. However, in most cases, the inflatable structure can only have one stable configuration, which is undesirable for robotic arms. This study proposes a novel inflatable structure that can be easily reconfigured into multiple stable configurations, even with single-body inflation. In the proposed mechanism, the structure length can be freely adjusted, and its respective joints can be set in the desired directions to facilitate the reconfiguration of its pose. An additional advantage of the proposed mechanism is that it can withstand external forces as well as its own weight. This study analyzes and experimentally validates the shape locking and load-carrying properties of the proposed mechanism. Further, the fabrication process and design guidelines for the proposed mechanism are presented. Through a suitable demonstration, the proposed mechanism is shown to exhibit multiple stable configurations and lock its poses.**

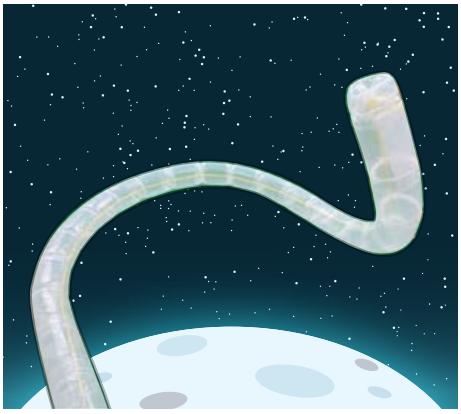

Fig. 1. Conceptual image of reconfigurable inflated soft arm (RISA) shape-locked in free space.

I. INTRODUCTION

Inflatable structures have been intensively studied owing to their numerous advantages, such as being light weight, low cost, and easy to package; moreover, they are easy to dispose and can interact safely with objects and live entities. These advantages of inflatable structures have been used for space mission applications [1]–[3] such as, inflatable habitats that can be packed in the spaceship [4], [5] and inflatable sunshields, antennas, concentrators and reflectors that can be inflated in a large scale [6]–[9]. However, despite the numerous advantages of such inflatable structures, their range of applications is generally limited to static structures, such as habitats and antennas. This is because an inflatable structure requires a large force corresponding to the internal pressure to deform it from its predefined shape; it then returns to its original stable configuration when the applied force is removed [10]. However, lowering the internal pressure is not useful because it may cause undesired deformation and buckling of the structure.

In the field of robotics, several studies have focused on building robots with inflatable structures. A soft growing robot, which is an everted inflated cylinder, can freely adjust its length at the tip by utilizing the advantage of a small volume of uninflated inner material [11]. Soft inflatable shells covering the exterior of rigid robots can increase the safety during interactive tasks [12]. Further, an untethered isoperimetric soft robot can reconfigure its truss-like structure by distributing the length of each inflated link using the roller module at the vertex and exploring rough terrain [13].

In addition to these robots, inflatable robotic arms have been intensively studied [14]–[21]. Inflatable beams have been employed on their robotic arms while achieving weight reduction and safe interaction. Among these robots, there are those whose joints are based on a rigid mechanism with only the links being inflatable beams [14], [22]. However, the joint mechanism sacrifices the inherent advantages of the inflatable structure owing to the robotic arm being complex and heavy. Thus, studies were then focused on a single-body inflatable robotic arm with all links and joints being connected and inflatable to preserve the advantages of the inflatable structure [23], [24]. As these inflatable robotic arms had only one inflation channel, the internal pressure was the same. Therefore, they changed the geometric shape of the joint to reduce the bending stiffness of the inflated joint.

Geometric shapes that reduce the stiffness of an inflatable structure are conventionally considered a problematic structural instability to be avoided in the field of inflatable structures. This is because an inflatable structure must stably withstand large forces in conventional applications. Therefore, several studies have been conducted on methods to stabilize them. Examples of such structural instability in an inflatable structure include the instability of a scientific balloon [25], lobed column [26], vacuum chamber [27], deployable reflectors [28], and inflatable antennas [29]. How-

This research was supported in part by a grant of the Korea Health Technology R&D Project through the Korea Health Industry Development Institute (KHIDI), funded by the Ministry of Health & Welfare, Republic of Korea (grant number : HI22C079600) and in part by the National Research Foundation of Korea under Grant NRF-2020R1A2C200416913. (*Corresponding author: Jee-Hwan Ryu.*)

[1] Nam Gyun Kim is with the Robotics Program, Korea Advanced Institute of Science and Technology (KAIST), Daejeon, Republic of Korea nam96bird@kaist.ac.kr

[2] Jee-Hwan Ryu is with the Department of Civil and Environmental Engineering, Korea Advanced Institute of Science and Technology (KAIST), Daejeon, Republic of Korea jhryu@kaist.ac.kr

ever, as mentioned earlier, in the case of a robotic arm, this structural instability may be desirable in certain situations, such as lowering the bending stiffness of the joint.

This study exploits the structural instability of a lobed cylindrical inflatable structure and converts its adverse effects into additional advantages for an inflatable robotic arm. By utilizing the structural instability, a novel single-body inflated soft arm referred to as reconfigurable inflated soft arm (RISA) is proposed. RISA can achieve infinite stable configurations without the use of actuators, in contrast to most other conventional single-body inflatable robot arms that can only have one stable and straight configuration. Fig 1 shows a conceptual image of the RISA shape locked in free space. The RISA can passively maintain its pose by using its structural moment balance. Further, it can withstand its own weight as well as external forces while passively locking its pose. In addition, RISA is essentially an everted cylinder, thereby facilitating free adjustment of its length by the growth mechanism of the soft growing robot. Furthermore, RISA can enhance its locking capability by increasing the internal pressure without disturbing its shape-locked pose because its shape-locking is based on a structural moment balance that is independent of pressure.

This study proposes, for the first time, a single-body inflated soft arm with an infinitely stable configuration. The shape-locking and load-carrying features of the proposed mechanism are analyzed and experimentally validated using moment equilibrium. Further, the fabrication process and a few guidelines that must be considered when designing the proposed mechanism are presented. Moreover, through a suitable demonstration, it is confirmed that the proposed mechanism can be reconfigured into various poses even after inflation, and can be shape-locked while withstanding its own weight.

The remainder of this paper is organized as follows: Section 2 describes the concept of RISA. Section 3 presents an analysis of the behaviors and features of RISA. Further, Section 4 discusses the fabrication methods, experimental results, design guidelines, and demonstration results of RISA. Finally, Section 5 concludes the paper.

II. Concept of RISA

Highly curved lobes formed by thin membranes inflating between stiff inelastic tapes are often referred to as lobed design in the field of inflatable structures [30]. This design offers advantages such as long duration, high pressure-carrying efficiency, and static determination of stress distribution. Despite its many attractive characteristics, the fundamental structural instability of the lobed design restricts its applications. However, the instability of a lobed inflatable cylinder could be an additional benefit when applied to an everted cylinder.

Everted inflated cylinders, such as soft growing robots, normally have a considerably larger restoring moment than that generated by the inner material (tail). Therefore, even in the buckled configuration, the everted cylinder will be restored if a force is applied to restore or grow it. However, everted inflated cylinders with lobes can always have a buckled state in a stable manner and can even withstand certain forces. RISA is essentially an everted inflated cylinder with multiple load-carrying hoops at appropriate intervals. Load-carrying hoops, which have a smaller diameter than the cylinder, cause the cylinder to inflate with lobed joints and geometrically reduce the bending stiffness at the joints. Therefore, the lobed joint buckles first when a moment is applied to the cylinder, which results in the moment induced by the tail being greater than the restoring moment of the lobed part. Consequently, with only simple single-body inflation, RISA can have multiple stable configurations, lock the respective joints in both radial and circumferential directions, and withstand external forces.

III. Static Analysis

A. Self-restoring Moment of the Lobed Joints

The self-restoring moment is the internal moment that causes the inflated cylinder in a bent configuration to return to its original straight line because of its internal pressure. It can be derived according to the deflection angle using the work equation. The principle presented in [31] was considered in this study.

The work W performed by the system is represented as follows:

$$W = \int PdV = \int Md\theta, \tag{1}$$

where P denotes the internal pressure, V denotes the volume, M denotes the applied moment, and θ denotes the deflection angle. Assuming that the internal pressure of the cylinder is regulated as a constant value, the resulting self-restoring moment at deflection angle θ can be represented as follows:

$$M_{res} = -P \cdot \frac{dV(\theta)}{d\theta}. \tag{2}$$

Here, $V(\theta)$ is the volume as a function of the deflection angle, with the negative sign indicating that it acts opposite to the external moment. The volume change of the lobed joint can be derived in a similar manner by referring to Lennon and Pellegrino [26]. To avoid calculation complications, three conditions were assumed: the deformation of RISA occurs locally at the lobed joints; the circumferential hoop with the smallest diameter at the lobed joint maintains its circular shape in the buckling mode, and the length from the center of the end of the lobed joint to the center of the circumferential hoop is maintained during buckling, as illustrated in Fig. 2(a). Under these conditions, the volume change of the lobed joint can be obtained by using the same method as in [26]. The resulting restoring moment of the lobed cylinder is expressed as follows:

$$M_{res} = \frac{-PBh\theta}{24}\left[1 - \frac{3\pi B}{4h} \cdot \frac{cos\xi + \xi sin\xi}{sin\xi - \xi cos\xi}\right], \tag{3}$$

where B is the diameter of the circumferential hoop, h is the height of the lobed part, and ξ is the alternate angle that represents the convexity of the lobed part, as shown in Fig. 2(b).

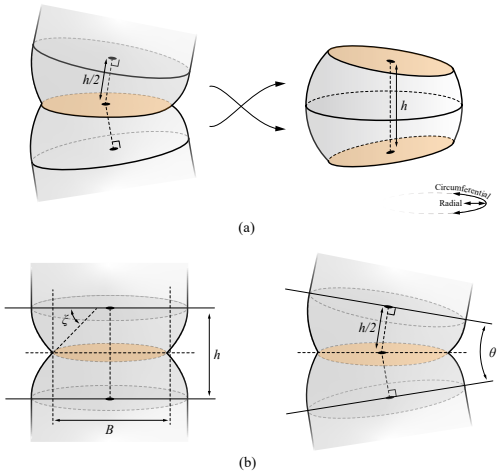

Fig. 2. Lobed joint of RISA in straight and buckled configurations. (a) Illustration of the assumption used to derive the volume change of RISA during buckling. (b) Parameters representing the shape of the lobes.

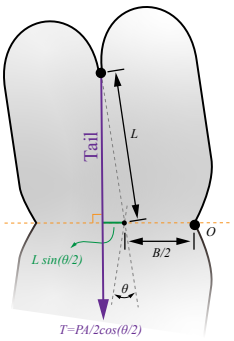

Fig. 3. Cross-section of the head segment of RISA in buckled configuration.

B. Effect of the Tail Tension

The inflated cylinders in the everted state exert a tension caused by the internal pressure on their inner material (tail), known as tail tension. In the case of a normal everted cylinder, the tail tension cannot generate a moment larger than the restoring moment unless the cylinder is already in the critical buckled state. However, for lobed everted cylinders, the moment due to the tail tension can be greater than the restoring moment, which is reduced by the lobed design. This condition causes RISA to be bent as a default and provides additional shape-locking capability against external forces. The tail moment generated by the tail tension from the geometric conditions of the RISA was calculated and directly compared with the restoring moment obtained in Section III-A. To simplify the calculation, the lobed joint was assumed to be fully collapsed to ensure that the center of the moment generated by the tail tension is at the end of the joint, similar to a hinge [10], with the tail at a right angle to the lobed joint, as shown in Fig. 3. The tail moment generated by tail tension T about the center of moment O can be expressed simply using small-angle approximations as follows:

$$M_{tail} = \frac{PA}{2}\left(\frac{B}{2} + \frac{L\theta}{2}\right), \tag{4}$$

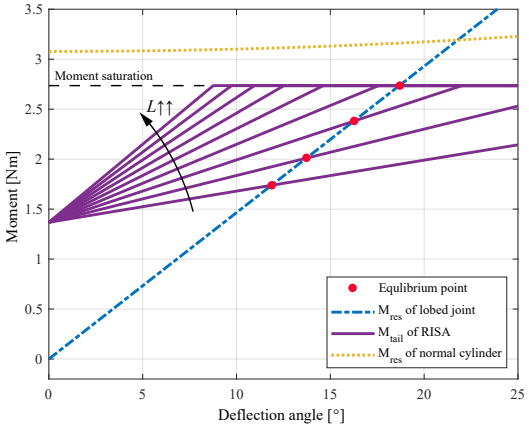

Fig. 4. Restoring and tail moments of RISA according to the deflection angle of the head segment. (P = 10 kPa, B = 0.0764 m, r = 0.0477 m, A = 0.0072 m^2, ξ = 1.5708 rad)

where P is the internal pressure, A is the circular cross-sectional area of the tip, B is the diameter of the circumferential hoop, L is the length of the head segment, and θ is the deflection angle between two segments. The head segment bends until M_{tail} is in equilibrium with M_{res}. The resulting deformation angle of the head segment can be calculated at the intersection of the two graphs, as indicated by the red dots in Fig. 4. Moment saturation occurs when the tail can no longer move far from the origin of the moment, owing to the circumferential hoop, even if the deflection angle increases.

Similar to the head segment, the grown body segments buckle themselves, and each body segment remains at a constant length L_b and maintains its predetermined direction. The shape-locked curve of the body segments in the two-dimensional plane is illustrated by the red dotted box in Fig. 5(a), comprising fully bent body segments. A similar calculation for the tail moment with the head segment can also be applied to the tail moment of the body segment. Considering that the tail is always biased toward one side of the curve, the tail moment of the fully bent body segment can be simply obtained as

$$M_{tail,b} = \frac{1}{2}PAB. \tag{5}$$

By substituting Eqs. (3) and (5), the resulting deformation angle θ_b of the fully bent body segment is obtained. The value of deformation angle θ_b depends only on the shape parameters and not on the internal pressure, because both the restoring moment and tail moment were directly proportional to the internal pressure. Consequently, the equivalent maximum curvature κ of the body segments can also be calculated.

$$\kappa \approx \frac{L_b}{\theta_b}. \tag{6}$$

Notably, in the plane configuration, inflection can also occur in the body segments, as indicated by the blue dotted box in Fig. 5(b). By passing through this inflection point, RISA can exhibit completely opposite directional curves.

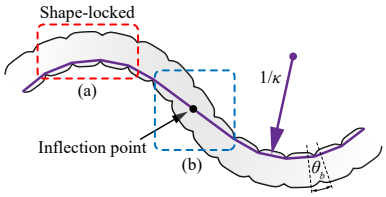

Fig. 5. Illustration of the body segments including (a) shape-locked curve and (b) inflection section.

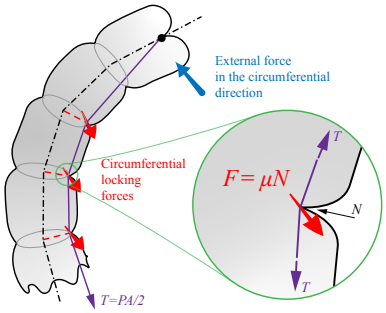

Fig. 6. Circumferential locking against the external force

C. Circumferential Locking by Friction

In addition to the analysis of RISA in the two-dimensional plane, the behavior of RISA in three-dimensional space with circumferential locking by friction can also be explained. Circumferential locking prevents deflection owing to self-weights and external forces in the circumferential direction and is achieved through friction between the tail and inner wall of the lobed part. Fig. 6 illustrates circumferential locking against an external force. The vertical reaction force N can be expressed using the tail tension T and the deformed angle of the fully bent body segment θ_b. Therefore, the maximum force of static friction F_s between the tail and inner wall can be obtained using the following equation:

$$F_s = \mu_s \cdot N = \mu_s P A \sin\frac{\theta_b}{2}, \tag{7}$$

where μ_s denotes the coefficient of static friction, P denotes the internal pressure, and A denotes the circular cross-sectional area of the tip. The internal pressure can be increased or a material with a high static friction coefficient may be chosen to obtain a large circumferential locking capability. Consequently, RISA can lock its shape in both the radial and circumferential directions owing to the moment balance and frictional force from the tail. Therefore, RISA can achieve and maintain complex postures while withstanding external forces.

D. Bouncing Behavior

During growth, a bouncing behavior of RISA was observed, caused by a change in the effective tip area when passing through the circumferential hoop during growth. Fig. 7(a) shows the bouncing behavior of RISA. When the distal end of the head segment meets the lobed part during growth (red circle), the tail tension decreases according to the smaller effective area of the tip. This reduced tail

(a)

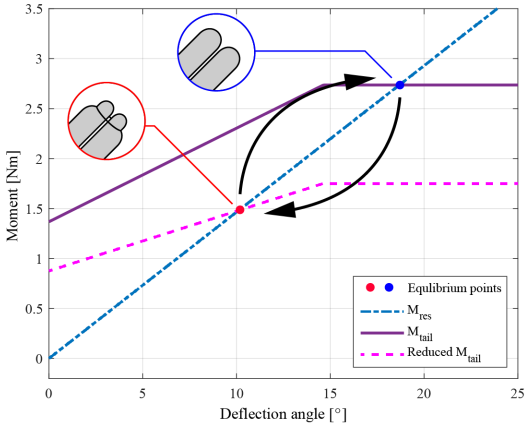

(b)

Fig. 7. Bouncing behavior of RISA. (a) RISA with a reduced effective tip area exhibits a lower curvature than the normal. (b) When the distal end of RISA meets the circumferential hoop, the tail moment and the corresponding deflection angle become smaller. (P = 10 kPa, B = 0.0764 m, r = 0.0477 m, A = 0.0072 m^2, ξ = 1.5708 rad, L = 0.3 m)

tension generates a smaller corresponding moment, M_{tail} and slightly lowers the entire curvature of RISA. Fig. 7(b) explains the bouncing behavior with corresponding moments and deformation angles. When the head segment encounters a hoop, M_{tail} drops and the joint angle decreases until it is in equilibrium with M_{res} (red dot). After passing through the hoop, M_{tail} returns to its original value, and the joint angle increases until it is in equilibrium with M_{res} (blue dot). This bouncing behavior is more pronounced as the ratio between the diameter of the lobed joint and that of the body increases.

IV. Experimental Results

A. Fabrication

A low-density polyethylene (LDPE) vinyl cylinder with diameter and thickness of 95 and 0.15 mm, respectively, was chosen for all experiments. The lobed design was realized using an inelastic string as a circumferential hoop. Fig. 8 shows the process of fabrication of RISA. Another layer of vinyl was placed on the part where the lobed joint was formed (Fig. 8(a–c)). Subsequently, strings were tied between the two vinyl gaps to create circumferential hoops (Fig. 8(d–f)). Finally, the cylinder and formed lobed joints were inflated (Fig. 8(g–h)).

B. Self-restoring Moment of the Lobed Cylinder

An experiment on self-restoring moment was conducted to demonstrate the lower banding stiffness of the lobed cylinder than the normal cylinder. The experiment was

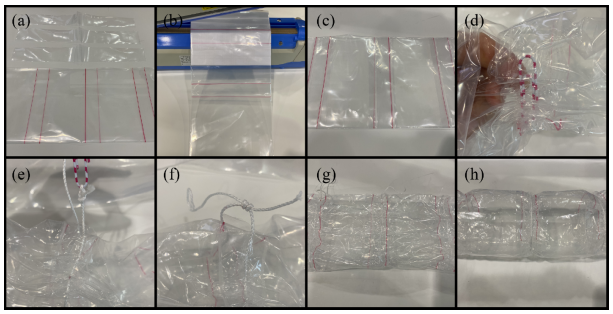

Fig. 8. Fabrication process of RISA.

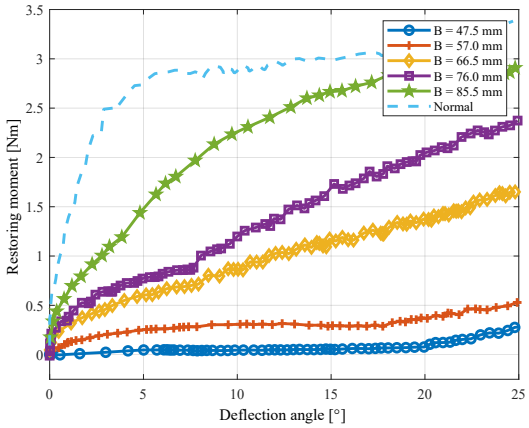

Fig. 9. Restoring moment of the lobed cylinder according to the deflection angle at six different hoop diameters in 10 kPa.

performed by applying an external moment to the cylinder, while simultaneously measuring the moment and deflection angle. The internal pressure was maintained at 10 kPa. Six experiments were conducted with circumferential hoops of different diameters, including a normal cylinder. Fig. 9 shows the restoring moment of lobed joints as a function of the deflection angle. The lobed cylinders produced a lower restoring moment than a normal cylinder. In addition, the trends for the lobed cylinder were almost linear for a wide range of deflection angles, whereas that for the normal cylinder increased sharply and settled because of the collapse property of the conventional inflated cylinder. Although the experiment was sufficient to confirm that a smaller circumferential hoop results in the lower bending stiffness of a lobed cylinder, it could not validate the model because the assumption mentioned in Section III was violated during the experiment because of the absence of a tail. A model validation experiment that considers all the assumptions of the analysis will be conducted in future research.

C. Locking Capability

To demonstrate the promising load-carrying capabilities of RISA, a locking capability experiment was conducted, wherein RISA resisted the external moment in the radial and circumferential directions. To measure the radial locking capability, the external moment was gradually increased in

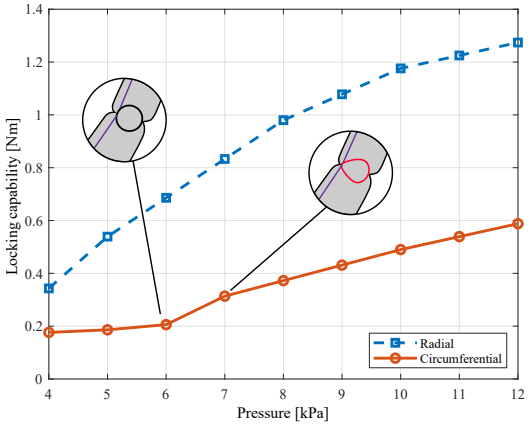

Fig. 10. Locking capability of RISA with a hoop diameter of 76 mm against radial and circumferential external moments.

the radial direction until the tail detached from the inner wall of the RISA. Similarly, to measure the circumferential direction locking capability, the external moment was gradually increased in the circumferential direction until the tail began sliding along the inner wall of RISA. Nine experiments were conducted at a pressure interval of 1 kPa for each case. Fig. 10 shows the external moment that RISA with a hoop diameter of 76 mm can withstand. A large load-carrying capability in the radial direction was observed when the internal pressure was high. However, even with high internal pressure, circumferential locking did not dramatically increase. This can be attributed to the low coefficient of friction of the LDPE. Further, in the region of 6–7 kPa, the circumferential hoop was deformed by tail tension; this violated the assumption of the analysis in Section III. However, it resulted in an additional locking force in the circumferential direction and higher stiffness, as shown in Fig. 10.

D. Design Guidelines for RISA

1) Diameter of circumferential hoop: As shown in previous experimental results (Fig. 9), the smaller the diameter of the circumferential hoop, the lower the restoring moment of the lobed joint. However, this result should not be used as it is to properly obtain the high deflection angle of the body segment. The fact that the maximum moment arm of the tail moment is constrained by the diameter of the circumferential hoop must be considered. Therefore, an experiment was conducted to obtain the deflection angle of the body segment based on the circumferential hoop diameter. The resulting deflection angles of the body segment were measured while varying the circumferential hoop diameter. As evident in Fig. 11, the deflection angle of the body segment decreased with increase in the hoop diameter, and after a diameter of 76 mm, the resulting deflection angle of the body segment decreased drastically.

The bouncing behavior must also be considered when designing the diameter of the circumferential hoop. Usually, bouncing behavior adversely affects the performance of

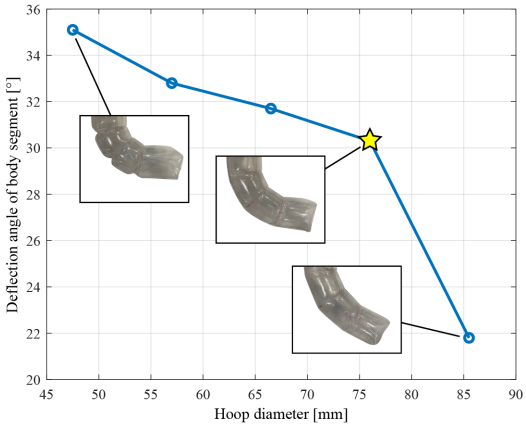

Fig. 11. Deflection angle of the body segment according to the diameter of the circumferential hoop.

RISA. Moreover, it became more intense with decrease in the hoop diameter, as discussed in Section III-D. To minimize adverse bouncing behavior while achieving a sufficiently high curvature, a hoop diameter of 76 mm was selected for the prototype.

2) Interval of lobed joints: As discussed in Section III-B, the resultant equivalent maximum curvature of RISA can be determined by both the deflection angle and length of the body segment. The length of the body segment can be different even in one RISA if desired. In this study, the length of the body segment was designed as a constant value to show that the equivalent maximum curvature discussed in Section III-B is formed. Because the deflection angle of the body segment was previously set to be considerably large, the length of the body segment was considered as a relatively long constant length (100 mm). The curvature of a prototype RISA with a hoop diameter of 76 mm and body segment length of 100 mm is shown in Fig. 12. The resultant curvature near the tip of the RISA was similar to the calculated equivalent maximum curvature; however, the tail tension decreased as it transmitted toward the base owing to the friction between the outerwall and the tail. Thus, the corresponding curvature also decreased, and consequently, RISA showed a spiral-shaped curve.

As discussed in Section III-B, curvature is decoupled from pressure. Therefore, the curvature was not attenuated even at higher pressures. This enabled the application of more pressure to stiffen the shape-locking without deforming the curvature. However, this also implies that the desired curvature should be considered in the manufacturing step because adjusting the resultant curvature is not possible.

E. Complex Pose Demonstration

The complex poses were demonstrated by manually reconfiguring the RISA while fixing the tail position. Fig. 13 shows the reconfiguration of RISA into various complex poses. RISA is a single inflated body; however, it can have multiple shape-locked stable poses because the moment balance between the inflated lobed joint and the tail is always achieved regardless of the pose.

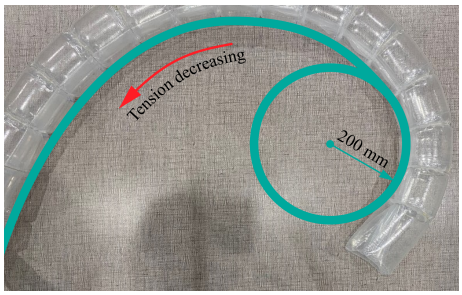

Fig. 12. Resultant curvature of RISA with a hoop diameter of 76 mm and body segment length of 100 mm.

Fig. 13. Complex pose demonstration of RISA.

V. Conclusion

This study proposed a novel inflated soft arm referred to as RISA, which can have multiple stable configurations, even with a single inflated body, and can withstand external forces in both the radial and circumferential directions. Therefore, RISA can exhibit diverse poses while withstanding its own weight. The moment equilibrium, which enables RISA to be shape-locked and carry payloads, was analyzed and experimentally investigated. Further, the special feature of RISA, bouncing behavior, was discussed and considered in the design guidelines. The design guidelines for RISA, including the hoop diameter and interval of lobed joints, were provided. Finally, the reconfiguration of RISA into complex poses was demonstrated. The simplicity of RISA, wherein a single inflated body can be reconfigured into multiple poses, provides additional degrees of freedom in terms of hardware design. Moreover, RISA can be applied as a component of soft robots, as well as any inflatable structure that needs to lock its poses while withstanding external forces. In future work, RISA will be developed as an actuated soft robotic manipulator that has a large payload capacity with a lower actuation force owing to passive shape-locking, while retaining the inherent advantages of the inflatable structure.

REFERENCES

[1] C. Cassapakis and M. Thomas, "Inflatable structures technology development overview," in *Space programs and technologies conference*, 1995, p. 3738.

[2] R. Freeland, G. Bilyeu, G. Veal, and M. Mikulas, "Inflatable deployable space structures technology summary," 1998.

[3] D. Cadogan and S. Scarborough, "Rigidizable materials for use in gossamer space inflatable structures," in *19th AIAA Applied Aerodynamics Conference*, 2001, p. 1417.

[4] D. Cadogan, J. Stein, and M. Grahne, "Inflatable composite habitat structures for lunar and mars exploration," *Acta Astronautica*, vol. 44, no. 7-12, pp. 399–406, 1999.

[5] S. Veldman and C. Vermeeren, "Inflatable structures in aerospace engineering-an overview," *Spacecraft Structures, Materials and Mechanical Testing*, vol. 468, p. 93, 2001.

[6] M. Bernasconi and S. Köse, "The space-rigidised thermal shield for the esa far-infrared space telescope(first)," in *ESA, Third European Symposium on Space Thermal Control and Life Support Systems p 165-173(SEE N 89-28214 22-54)*, 1988.

[7] R. Freeland, G. Bilyeu, G. Veal, M. Steiner, and D. Carson, "Large inflatable deployable antenna flight experiment results," *Acta Astronautica*, vol. 41, no. 4-10, pp. 267–277, 1997.

[8] J. Bagby and S. Schwartz, "Rigidized inflatable solar energy concentrators, 1 august 1963-25 december 1964," Tech. Rep., 1965.

[9] G. Reibaldi and M. Bernasconi, "Quasat program: the esa reflector," *Acta astronautica*, vol. 15, no. 3, pp. 181–187, 1987.

[10] R. Comer and S. Levy, "Deflections of an inflated circular-cylindrical cantilever beam," *AIAA journal*, vol. 1, no. 7, pp. 1652–1655, 1963.

[11] E. W. Hawkes, L. H. Blumenschein, J. D. Greer, and A. M. Okamura, "A soft robot that navigates its environment through growth," *Science Robotics*, vol. 2, no. 8, p. eaan3028, 2017.

[12] T. Kim, S. J. Yoon, and Y.-L. Park, "Soft inflatable sensing modules for safe and interactive robots," *IEEE Robotics and Automation Letters*, vol. 3, no. 4, pp. 3216–3223, 2018.

[13] N. S. Usevitch, Z. M. Hammond, M. Schwager, A. M. Okamura, E. W. Hawkes, and S. Follmer, "An untethered isoperimetric soft robot," *Science Robotics*, vol. 5, no. 40, p. eaaz0492, 2020.

[14] N. Salomonski, M. Shoham, and G. Grossman, "Light robot arm based on inflatable structure," *CIRP annals*, vol. 44, no. 1, pp. 87–90, 1995.

[15] S. Sanan, M. H. Ornstein, and C. G. Atkeson, "Physical human interaction for an inflatable manipulator," in *2011 annual international conference of the IEEE engineering in medicine and biology society*. IEEE, 2011, pp. 7401–7404.

[16] S. Voisembert, N. Mechbal, A. Riwan, and A. Aoussat, "Design of a novel long-range inflatable robotic arm: Manufacturing and numerical evaluation of the joints and actuation," *Journal of Mechanisms and Robotics*, vol. 5, no. 4, p. 045001, 2013.

[17] R. Qi, A. Khajepour, W. W. Melek, T. L. Lam, and Y. Xu, "Design, kinematics, and control of a multijoint soft inflatable arm for human-safe interaction," *IEEE Transactions on Robotics*, vol. 33, no. 3, pp. 594–609, 2017.

[18] J. M. À. Palacio, A. Riwan, N. Mechbal, E. Monteiro, and S. Voisembert, "A novel inflatable actuator for inflatable robotic arms," in *2017 IEEE International Conference on Advanced Intelligent Mechatronics (AIM)*. IEEE, 2017, pp. 88–93.

[19] H.-J. Kim, A. Kawamura, Y. Nishioka, and S. Kawamura, "Mechanical design and control of inflatable robotic arms for high positioning accuracy," *Advanced Robotics*, vol. 32, no. 2, pp. 89–104, 2018.

[20] P. Ohta, L. Valle, J. King, K. Low, J. Yi, C. G. Atkeson, and Y.-L. Park, "Design of a lightweight soft robotic arm using pneumatic artificial muscles and inflatable sleeves," *Soft robotics*, vol. 5, no. 2, pp. 204–215, 2018.

[21] P. Palmieri, M. Gaidano, M. Troise, L. Salamina, A. Ruggeri, and S. Mauro, "A deployable and inflatable robotic arm concept for aerospace applications," in *2021 IEEE 8th International Workshop on Metrology for AeroSpace (MetroAeroSpace)*. IEEE, 2021, pp. 453–458.

[22] S. Sanan, J. B. Moidel, and C. G. Atkeson, "Robots with inflatable links," in *2009 IEEE/RSJ International Conference on Intelligent Robots and Systems*. IEEE, 2009, pp. 4331–4336.

[23] S. Voisembert, A. Riwan, N. Mechbal, and A. Barraco, "A novel inflatable robot with constant and continuous volume," in *2011 IEEE International Conference on Robotics and Automation*. IEEE, 2011, pp. 5843–5848.

[24] M. Hofer, J. Zughaibi, and R. D'Andrea, "Design and control of an inflatable spherical robotic arm for pick and place applications," in *Actuators*, vol. 10, no. 11. MDPI, 2021, p. 299.

[25] C. Calladine, "Stability of the 'endeavour'balloon," in *Studies in Applied Mechanics*. Elsevier, 1988, vol. 19, pp. 133–149.

[26] B. Lennon and S. Pellegrino, "Stability of lobed inflatable structures," in *41st Structures, Structural Dynamics, and Materials Conference and Exhibit*, 2000, p. 1728.

[27] S. A. Barton, "Stability analysis of an inflatable vacuum chamber," *Journal of Applied Mechanics*, vol. 75, no. 4, 2008.

[28] C. Wang, Z. Xia, and H. Tan, "Initial shape design and stability analysis of rib for inflatable deployable reflector," *AIAA Journal*, vol. 53, no. 2, pp. 486–492, 2015.

[29] T. Liu, X. Wang, X. Qiu, and X. Zhang, "Theoretical study on the parameter sensitivity over the mechanical states of inflatable membrane antenna," *Aerospace Science and Technology*, vol. 102, p. 105843, 2020.

[30] M. Pagitz, Y. Xu, and S. Pellegrino, "Stability of lobed balloons," *Advances in space research*, vol. 37, no. 11, pp. 2059–2069, 2006.

[31] C. R. Nesler, T. A. Swift, and E. J. Rouse, "Initial design and experimental evaluation of a pneumatic interference actuator," *Soft robotics*, vol. 5, no. 2, pp. 138–148, 2018.